

CrossMark
click for updatesCite this: *RSC Adv.*, 2014, 4, 40828

Photocatalytic degradation of phenol by the heterogeneous Fe₃O₄ nanoparticles and oxalate complex system

Piao Xu,^{ab} Guangming Zeng,^{*ab} Danlian Huang,^{*ab} Liang Liu,^{ab} Cui Lai,^{ab} Ming Chen,^{ab} Chen Zhang,^{ab} Xiaoxiao He,^{ab} Mingyong Lai^{ab} and Yibin He^{ab}

A novel approach for the removal of phenol by an advanced oxidation process using Fe₃O₄ nanoparticles (NPs) and oxalate was proposed and investigated, and the influences of oxalate, Fe₃O₄ NPs and H₂O₂ dosage on the photodegradation of phenol were reported. No obvious difference is found between ultraviolet light and visible light exposure, confirmed potential photoactive roles of Fe₃O₄ NPs in the presence of oxalate under visible light. Furthermore, relatively high dependence of oxalate depletion was observed due to the initiation of the formation of the Fe(III)-carboxylate complexes for photodegradation via a photo-Fenton-like system. Our results also demonstrated that the photodegradation of phenol occurred by a radical mechanism accompanied with the formation of O₂^{•-} and [•]OH radicals, which was further accelerated by the exogenous addition of H₂O₂. All reactions followed the pseudo-first-order reaction kinetics. The half-life (*t*_{1/2}) of Fe₃O₄-oxalate and Fe₃O₄-oxalate-H₂O₂ in the system showed higher efficiencies of photo-Fenton-like degradation routes for phenol. The photo-Fenton-like systems showed a relatively high catalytic ability (>99.9%) in the removal of phenol at low phenol concentrations below 50 mg L⁻¹, indicating its potential application in the treatment of low concentration wastewater. The results have demonstrated the feasibility of Fe₃O₄ NPs as potential heterogeneous photo-Fenton photocatalysts for organic contaminants decontamination in industrial wastewater.

Received 19th June 2014
Accepted 31st July 2014

DOI: 10.1039/c4ra05996d

www.rsc.org/advances

1. Introduction

The efficient treatment of industrial wastewaters and contaminated drinking water sources has become of immediate importance that is facing ever increasing population. Phenol and its derivatives are among the most potential pollutants discharged from various industries, such as coal gasification, polymeric resin production, oil refining, coking plants, paper mill, herbicides and fungicides production.^{1,2} Traditional methods, such as solvent extraction, activated carbon adsorption, and common chemical oxidation often suffer from serious drawbacks including high cost or formation of hazardous by-products.^{3,4} For example, biological decontamination by chlorination method may result in the formation of more toxic chlorinated compounds during the conversion process.

It has, therefore, gained much attention owing to the urgent need for a clean and comfortable environment. Heterogeneous photocatalysis is one of a promising method for the elimination of toxic and bio-resistant organic compounds by transforming

them into innocuous species, which has been widely applied in the removal of organic pollutants in wastewater.⁵⁻⁷ Various photocatalysts have been developed in the past decades, such as TiO₂, ZnO, CdS, WO₃, and ZnS, demonstrating its high efficiency in degradation of a wide range of refractory organic pollutants into innocuous carbon dioxide and water under UV irradiation.⁸⁻¹⁰ However, limited efficiency and high cost in the use of irradiated energy limited the practical applications of heterogeneous photocatalysis. Considerable efforts have been made to enhance photocatalytic activity, such as decreasing photocatalyst size to increase surface area, combining photocatalyst with some novel metal nanoparticles, and increasing hole concentration through doping.^{11,12}

In recent years, the utilization of iron oxide nanoparticles (NPs) with novel properties and functions has been widely studied due to their nano-range size, high surface area to volume ratios and superparamagnetism.¹³⁻¹⁶ Most of iron oxides show semiconductor properties with narrow band gap (2.0–2.3 eV) and are photoactive under solar irradiation as photocatalysts absorbing visible light.^{7,17,18} For example, Fe₂O₃ with band-gap of 2.2 eV is an interesting n-type semiconducting material and a suitable candidate for photodegradation under visible light condition. Moreover, iron oxide containing Fenton-like heterogeneous photocatalysis has been widely reported in many advanced oxidation

^aCollege of Environmental Science and Engineering, Hunan University, Changsha 410082, PR China. E-mail: zgming@hnu.edu.cn; huangdanlian@hnu.edu.cn; Fax: +86-731-88823701; Tel: +86-731-88822754

^bKey Laboratory of Environmental Biology and Pollution Control (Hunan University), Ministry of Education, Changsha 410082, PR China

processes, but limited photocatalysis is frequently encountered because of the electron–hole charge recombination at the oxide surface, as fast as within nanoseconds.^{19,20} Accordingly, the mutual characterization of Fenton-reaction is the generation of hydroxyl radicals ($\cdot\text{OH}$), very powerful and active radicals with high oxidative capacity (reduction potential of $\cdot\text{OH}$ $E_0 = 2.8$ V), which can react with almost all organic pollutants, yielding dehydrogenated or hydroxylated derivatives through a multistep process.²¹ Thus, sufficient H_2O_2 have to be added to make the system efficient with $\cdot\text{OH}$ formation, resulting in the costly consumption of H_2O_2 . As an alternative, a photo-Fenton-like system based on the iron oxides and polycarboxylic acids, such as oxalate, has been set up with the formation of $\cdot\text{OH}$ without the exogenous addition of H_2O_2 .^{22,23} However, the effect of oxalate on the heterogeneous photodegradation of phenol in the presence of Fe_3O_4 nanoparticles has been scarcely studied.

In this study, we investigated phenol degradation by a Fe_3O_4 –oxalate based photo-Fenton-like system. Parameters affecting photodegradation process, such as pH, dosage of oxalate, Fe_3O_4 NPs and H_2O_2 , and phenol concentration were examined. Special attention has been given to the mechanistic insight into the photodegradation of phenol accompanied with the formation of reactive radicals. The results obtained in this study may shed some light on the possible route of phenol removal *via* photo-Fenton-like oxidation mechanism.

2. Experimental section

2.1. Chemicals

Iron chloride hexa-hydrate ($\text{FeCl}_3 \cdot 6\text{H}_2\text{O}$) and ferrous chloride tetra-hydrate $\text{FeCl}_2 \cdot 4\text{H}_2\text{O}$, 30% hydrogen peroxide, phenol and ethylene glycol were of analytical grade. Ultrapure water was used for the preparation of all the solutions throughout this study. Fe_3O_4 nanoparticles were prepared by the coprecipitation of $\text{FeCl}_3 \cdot 6\text{H}_2\text{O}$ and $\text{FeCl}_2 \cdot 4\text{H}_2\text{O}$ in ammonia solution according to our previous study.²⁴

2.2. Phenol photodegradation experiment

The phenol photodegradation experiment was implemented in a set of 250 mL conical flasks placed in a constant temperature oscillator with a vibration rate of 150 rpm at 303 K. Different operation conditions, such as pH value, Fe_3O_4 NPs dosage, oxalate and hydrogen peroxide dosage and initial phenol concentration were investigated in the batch experiments. Solutions (100 mL) with the desired concentration of phenol (10–300 mg L^{-1}) and the given oxalate concentrations (0–8.8 mM) at desired pH value (2.0–9.0) were fed into the reactor, and then, Fe_3O_4 NPs (ranging from 0.1–4.0 g L^{-1}) and H_2O_2 (0–2.35 mM) were simultaneously added. The initial pH of the solution was adjusted to the desired value ranging from 2.0 to 9.0 by adding a small quantity of 0.1 M HCl or NaOH solution. All the experiments were carried out in triplicate and data presented were the mean values from these independent experiments.

2.3. Characterization of the Fe_3O_4 nanoparticles

The morphologies of Fe_3O_4 NPs were characterized by a field emission scanning electron microscope (FESEM, JSM 6700F), equipped with energy dispersive spectroscopy (EDS, EDAX Genesis XM-2) after gold plating at an accelerating voltage of 20 kV for 30 s. The particle size of the Fe_3O_4 NPs was characterized by dynamic light scattering (DLS) using Zetasizer 3000HS (Malvern, UK) suspending in deionized water. The functional groups of Fe_3O_4 NPs were characterized by the corresponding Fourier transform infrared spectrophotometer (FTIR) spectra (Nicolet, Nexus-670) over the range 4000–400 cm^{-1} . The phase of prepared NPs was characterized by X-ray powder diffraction (XRD, Rigaku Rotaflex D/Max-C) performed by a monochromatized X-ray beam with nickel-filtered $\text{CuK}\alpha$ radiation.

2.4. Analytical procedures

At the given time intervals, the analytical samples were taken from the suspension filtered with a 0.45 μm Millipore filter and used for selected index detection immediately. The concentration of phenol was determined by spectrophotometric method at wavelength of 510 nm based on a chromogenic reaction between phenol and 4-aminoantipyrine in the presence of potassium ferricyanide *via* UV-vis spectrophotometer (UV-2550, Shimadzu).

Oxalate concentration residual in the solution was analyzed by HPLC (Agilent 1100) equipped with UV-vis variable wavelength detector (VWD) and reversed-phase C18 column. Phosphoric acid (0.15% v/v) was used as the mobile phase at a flow rate of 0.5 mL min^{-1} with the constant detection wave length at 210 nm. 10 μL of aqueous standard samples was injected into the liquid chromatograph. The column was maintained at 30 $^\circ\text{C}$.²⁵ Total Fe concentration was analyzed by atomic absorption spectrometry and ferrous ion (Fe^{2+}) concentration was analyzed by the ferrozine method as described by Paipa *et al.*²⁶ The production of superoxide anion ($\text{O}_2^{\cdot-}$) was measured with a Shimadzu 2550 UV-vis spectrophotometer at 530 nm according to our previous study.²⁷ The variation of hydroxyl radicals ($\cdot\text{OH}$) produced during the photocatalytic reactions was characterized as the absorbance variation at 532 nm, which detected in terms of thiobarbituric acid (TBA) method.²⁷

3. Results and discussion

3.1. Characterization of Fe_3O_4 nanoparticles

Fig. 1a and b show the SEM images of Fe_3O_4 NPs, and it can be seen that Fe_3O_4 NPs were evenly distributed with the homogeneity dimensional size. Meanwhile, EDS results shows in Fig. 1c demonstrate the enrichment of Fe and O element in Fe_3O_4 NPs. Fig. 1d shows that the size distribution of the sample is comparatively narrow, concentrated at diameters of approximately 12–20 nm. Most importantly, the prepared Fe_3O_4 NPs can be conveniently removed with an external magnet. Fig. 1e shows a digital photograph of the phenol solution with equally dispersed Fe_3O_4 NPs before and after magnetic separation using an external magnetic field. It is apparent that easy, fast separation of the Fe_3O_4 NPs can be realized during the experiments.

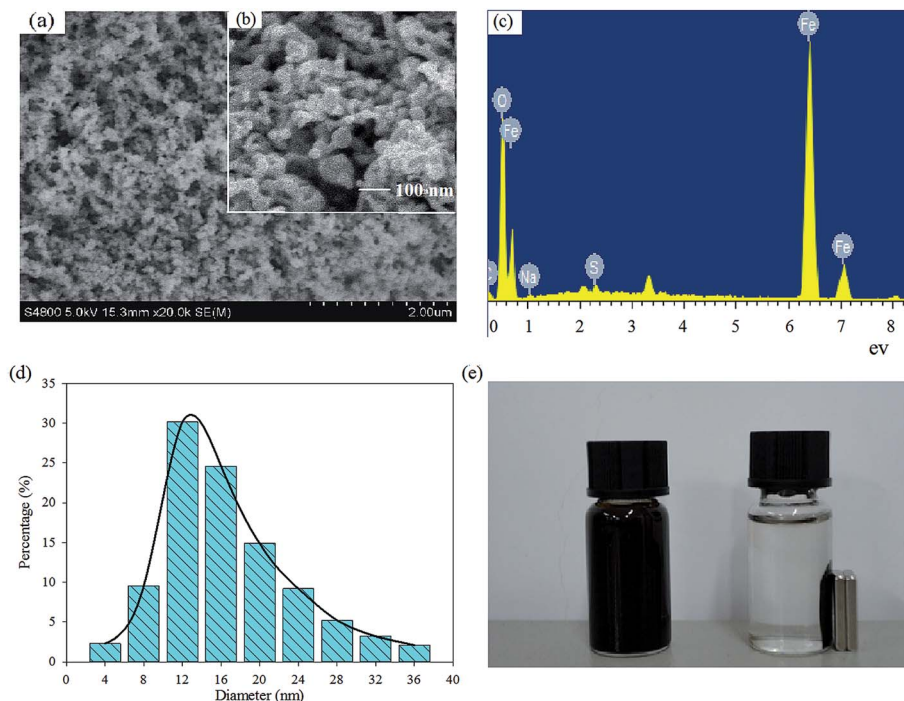


Fig. 1 Characterization of Fe_3O_4 nanoparticles via SEM images (a and b), EDS image (c), particle size analyzer, (d) and magnetic separation image (e).

Meanwhile, FTIR spectra of Fe_3O_4 NPs depicted two strong absorption bands at around 437 and 588 cm^{-1} , which demonstrated by vibrations of Fe–O bonds of Fe_3O_4 NPs. Meanwhile, the absorption bands at 3403 cm^{-1} may be ascribed to the presence of O–H at the surface of Fe_3O_4 NPs (Fig. 2a). Characteristic peaks at $2\theta = 31.4^\circ$, 35.4° and 55.2° are observed in Fig. 2b, which can be assigned to magnetite.

3.2. Effect of pH on phenol photodegradation

The role of pH on phenol removal was studied in the pH range 2.0–9.0 at phenol concentration of 100 mg L^{-1} (Fig. 3). Obviously, different tendencies are observed in various systems. For example, Fe_3O_4 NPs showed the highest removal efficiency at pH 5.0, while at pH 6.0 in $\text{Fe}_3\text{O}_4\text{-H}_2\text{O}_2$ system (0.1 mM). In the absence of oxalate, alkaline range is expected to favor the

formation of $\cdot\text{OH}$ radicals in $\text{Fe}_3\text{O}_4\text{-H}_2\text{O}_2$ system, thus enhancing the degradation ability.²⁸ However, for a solution initially containing 100 mg L^{-1} phenol, only about 6% of phenol is degraded by Fe_3O_4 NPs without the addition of oxalate and H_2O_2 at pH 2.0–3.0. Results indicated that adsorption mechanism played limited roles in phenol removal process.

Obviously, the initial pH value tends to be a very important factor affecting the photo-Fenton-like processes. A distinct enhancement of phenol removal is found in the acidic region than in the alkaline region in both $\text{Fe}_3\text{O}_4\text{-oxalate}$ (2.0 mM) and $\text{Fe}_3\text{O}_4\text{-oxalate-H}_2\text{O}_2$ systems. The maximum degradation occurred in the acidic pH range at 2.0–3.0 based on the fact that acid range could favor for the formation of $\text{Fe}^{\text{III}}(\text{C}_2\text{O}_4)_2^-$ and $\text{Fe}^{\text{III}}(\text{C}_2\text{O}_4)_3^{3-}$, initiating a series of photochemical reactions in $\text{Fe}_3\text{O}_4\text{-oxalate}$ and $\text{Fe}_3\text{O}_4\text{-oxalate-H}_2\text{O}_2$ systems.²⁹ In addition,

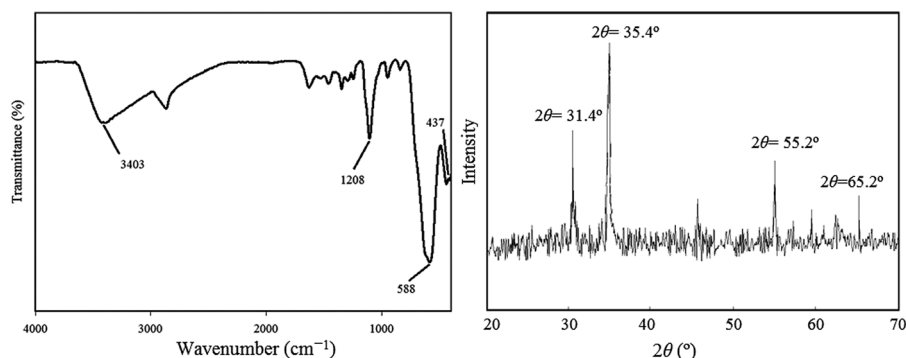


Fig. 2 Characterization of Fe_3O_4 nanoparticles via FTIR (a) and XRD (b).

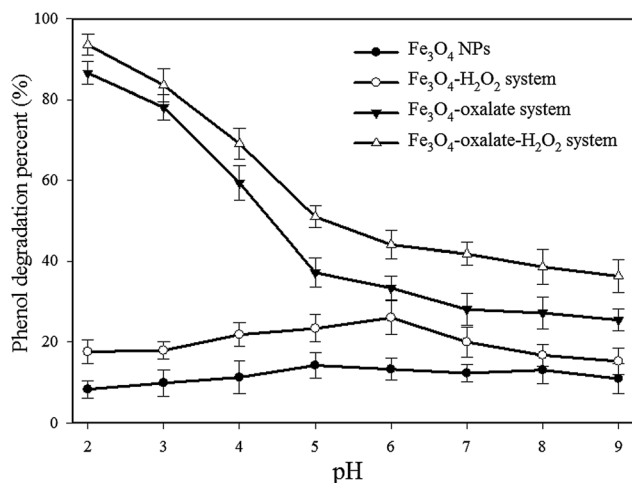


Fig. 3 Photodegradation behavior of phenol at different pH in various Fe_3O_4 -based degradation systems (time 4 h, Fe_3O_4 NPs 0.5 g L^{-1} , initial phenol concentration 100 mg L^{-1}).

phenol has a hydroxyl group in its molecular structure, which is negatively charged, the acidic solution favors adsorption of phenol onto the Fe_3O_4 surface, leading to the improvement of the degradation efficiency. A sharp depletion of phenol degradation above pH 4.0 implies that the operating conditions are at acid pH range, mainly due to the inactive formation of photoactive groups with the increasing pH. When the pH value increased to about 4.0–5.0, Fe(III) -oxalate species were mainly $\text{Fe(III)(C}_2\text{O}_4)^+$, which was low photoactive.³⁰ When the pH value was up to 6.0, the Fe^{3+} and Fe^{2+} almost cannot exist in the solution and the predominant Fe(III) and Fe(II) species were Fe(II)-OH and Fe(III)-OH as the precipitate, which may hardly be photoactive. Simultaneously, as pH was raised from 2.0 to 9.0, the phenol degradation efficiency decreased from 89.52% to 25.37% in Fe_3O_4 -oxalate system. Additionally, H_2O_2 as an oxidant was also applied to phenol degradation, and the degradation efficiency of phenol in the presence of neat oxalate, oxalate- H_2O_2 , FeCl_2 -oxalate- H_2O_2 and FeCl_3 - FeCl_2 -oxalate- H_2O_2 systems were also investigated to compare with the degradation ability of conventional methods (Table 1). As a result, relative low removal efficiency was found in oxalate, H_2O_2 and oxalate- H_2O_2 system. However, the phenol degradation promoted in FeCl_2 -oxalate- H_2O_2 and FeCl_3 - FeCl_2 -oxalate- H_2O_2 system, mainly due to the potential occurrence of photocatalytic reaction between Fe^{2+} and oxalate in the presence of H_2O_2 . Consequently, it was apparent that Fe_3O_4 -oxalate- H_2O_2 system showed the predominant degradation ability to phenol in the all tested degradation systems.

3.3. Effect of oxalate concentration on phenol photodegradation

Fig. 4 shows the effect of oxalate concentration (0–8.8 mM) on phenol photodegradation under ultraviolet light and visible light, respectively. It is apparent that no obvious difference is found between ultraviolet light and visible light exposure, which confirmed the potential photocatalytic roles of Fe_3O_4 NPs under solar irradiation in the presence of oxalate. Visible light is chosen as light source in the following study. Apparently, phenol removal was greatly promoted by the addition of oxalate from 0–2.2 mM. In the absence of oxalate, Fe_3O_4 NPs mainly acted as adsorbents and the photochemical transformation rate for organic pollutants on the surface of Fe_3O_4 NPs might be negligible under visible light.³¹ While in the presence of oxalate, the heterogeneous Fe_3O_4 -oxalate complex formed and a photo-Fenton-like system was set up, exhibiting a strong ligand-to-metal charge transformation ability.³¹ In this heterogeneous photo-Fenton-like system, Fe_3O_4 NPs mainly acted as a photocatalyst, while oxalic acid could be excited to generate electron-hole pairs.^{32,33} In previous work conducted by Liu *et al.*,³⁴ high photoactive groups $\text{Fe(C}_2\text{O}_4)_2^-$ and $\text{Fe(C}_2\text{O}_4)_3^{3-}$ have been detected in the iron oxide-oxalate system. Therefore, photodegradation efficiency is greatly enhanced in the presence of oxalate. However, excessive existence oxalate inhibited the photodegradation process. First of all, excessive oxalate would lead to the formation of a large amount of Fe^{3+} , which would inhibit the formation of H_2O_2 . In addition, excessive oxalate would occupy the adsorbed sites on the surface of Fe_3O_4 NPs and react competitively for $\cdot\text{OH}$.²⁹ Obviously, an optimal amount of oxalate achieving the best performance of the photodegradation of phenol was at the value of 2.2 mM.

From Fig. 4b, it was obvious that oxalate depleted during phenol degradation process, which was consistent with the previous hypothesis that oxalate participated in phenol photodegradation *via* a photo-Fenton-like system. Oxalate was strongly complexed with the Fe_3O_4 NPs with the formation of photoactive groups accelerating phenol photodegradation, contributing to the oxalate depletion. Significant correlations have been observed between oxalate depletion and phenol degradation efficiency, especially at the dietary range of oxalate concentration below 1.1 mM (Fig. 4b), based on the fact that oxalate participated in photo-Fenton-like system *via* a series of reactions for the formation of reactive radicals.

3.4. Possible mechanism involved in the photodegradation of phenol

Accordingly, the photochemical transformation could be improved when Fe_3O_4 NPs and oxalate set up a photo-Fenton-like system due to the formation of Fe(III) -carboxylate

Table 1 Phenol degradation efficiency in various oxalate and H_2O_2 containing systems

	Oxalate	H_2O_2	Oxalate- H_2O_2	FeCl_2 -oxalate- H_2O_2	FeCl_3 - FeCl_2 -oxalate- H_2O_2
pH 3	6.30%	20.35%	23.32%	58.98%	57.42%
pH 5	5.21%	25.76%	29.39%	64.91%	63.52%

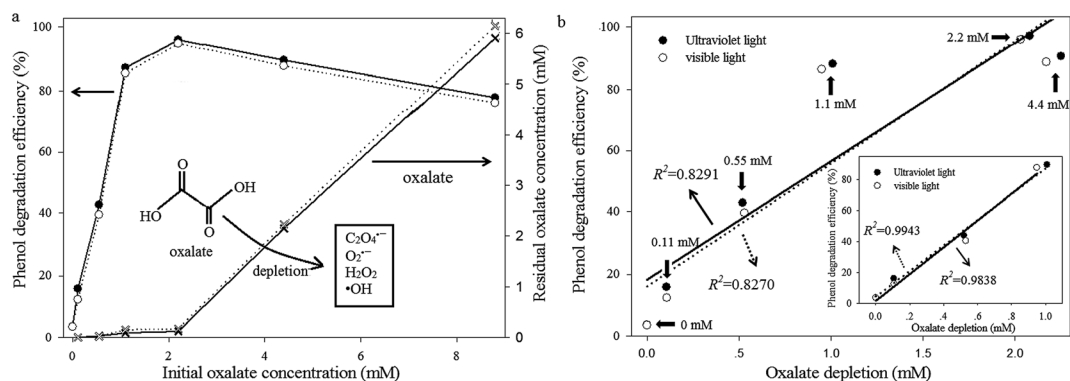
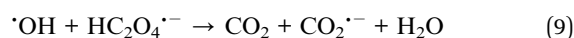
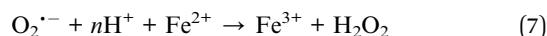
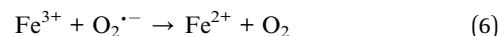
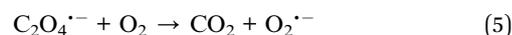
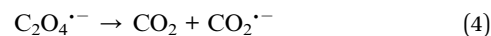
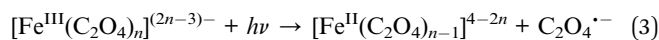
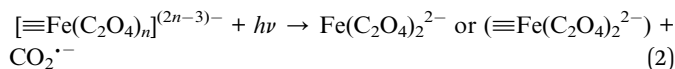
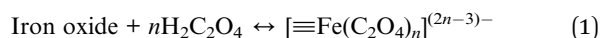


Fig. 4 (a) Phenol degradation in Fe_3O_4 NPs–oxalate system with various dosages of oxalate under ultraviolet (solid) and visible light (hollow); (b) correlation between oxalate depletion and phenol photodegradation (pH 2.0, Fe_3O_4 NPs 1.0 g L^{-1} , time 4 h, initial phenol concentration 100 mg L^{-1}).

complexes.^{19,20,26} First, oxalate is adsorbed by Fe_3O_4 NPs to form Fe_3O_4 –oxalate complexes, including $[Fe^{III}(C_2O_4)_n]^{(2n-3)-}$ or $[Fe^{II}(C_2O_4)_{n-1}]^{4-2n}$ (eqn (1)–(3)), which are much more photoactive than the other Fe^{3+} species, with the generation of oxalate radical $C_2O_4^{\cdot-}$ (eqn (3)). Then, oxygen trapped the electron from $C_2O_4^{\cdot-}$ and a rapid decarboxylation of $C_2O_4^{\cdot-}$ followed, with the formation of $O_2^{\cdot-}$ (eqn (5)). Under the acidic pH range, the formed $O_2^{\cdot-}$, further formed in $\cdot OOH$, *via* capturing a proton, which could further react with Fe^{2+} contributing to the generation of H_2O_2 (eqn (6) and (7)). H_2O_2 further reacts with Fe^{2+} to form $\cdot OH$ (eqn (8)), which generated in their redox-oxidize transformation process accompanied with the production and consumption of H_2O_2 , as described below, played a key role in the photodegradation course. Thereafter, organic pollutants will be attacked by $\cdot OH$ and mineralized efficiently in phenol photodegradation system. The illustration of the photodegradation mechanism is shown in Fig. 5.



In order to better understand the photodegradation mechanism, the changes in $O_2^{\cdot-}$ and $\cdot OH$ during the course of the reaction were measured to verify the formation and dependence

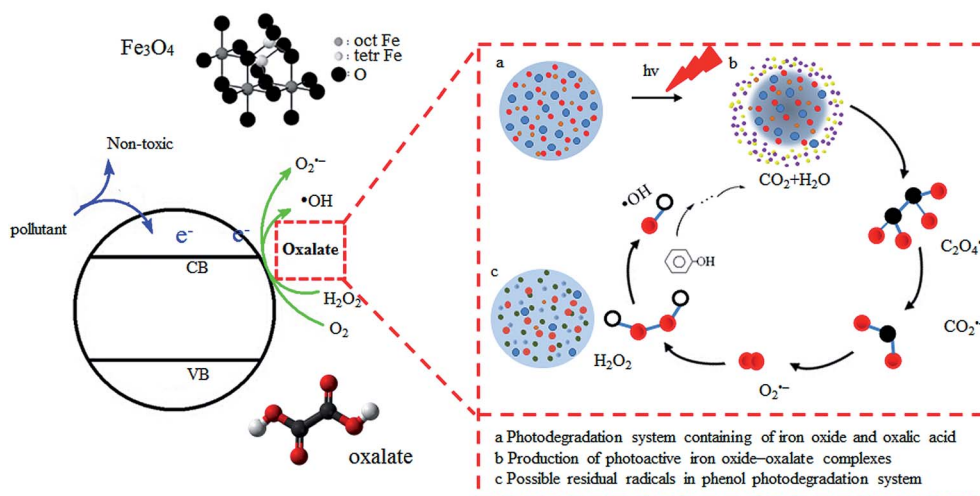


Fig. 5 Schematic diagram of photodegradation mechanism of Fe_3O_4 –oxalate system under visible light irradiation.

of $O_2^{\cdot-}$ and $\cdot OH$ radicals on the phenol photodegradation (Fig. 6). For both Fe_3O_4 -oxalate and Fe_3O_4 -oxalate- H_2O_2 system, the formation of $O_2^{\cdot-}$ and $\cdot OH$ radicals at the initial 5 min has been found, and the addition of exogenous H_2O_2 promoted the production of $O_2^{\cdot-}$ and $\cdot OH$. However, as the mobility and reactivity of radicals, it can be speculated that $O_2^{\cdot-}$ and $\cdot OH$ radicals, immediately after formation, leave the surface of Fe_3O_4 NPs and participated in the photodegradation reaction as shown in the above. As a result, a distinct depletion in both $O_2^{\cdot-}$ and $\cdot OH$ occurred at the end of the photodegradation process (Fig. 6).

3.5. Dynamic photodegradation of phenol

Fig. 7 shows the dynamics of phenol photodegradation by Fe_3O_4 NPs, Fe_3O_4 - H_2O_2 , Fe_3O_4 -oxalate and Fe_3O_4 -oxalate- H_2O_2 systems. It was found that the concentration of phenol remained almost unchanged after 180 min in the presence of Fe_3O_4 NPs. The observations demonstrated that the photocatalytic experiments occurred in a pure photocatalytic regime where Fe_3O_4 derived adsorption process could be neglected.

Significantly enhanced degradation rates of phenol were observed when oxalate was added into Fe_3O_4 nanoparticles. The behavior of phenol degradation by Fe_3O_4 -oxalate and Fe_3O_4 -oxalate- H_2O_2 was quite different from that by Fe_3O_4 or Fe_3O_4 - H_2O_2 ; for the former, reaction occurred similar to Fenton chemistry, through the participation of $\cdot OH$ in activating phenol degradation *via* Fenton-like oxidation process. One of the key stages in Fenton's processes is the generation of the oxidizing species, such as $\cdot OH$, by initiating of H_2O_2 decomposition.²⁵ The rate constants corresponding to $\cdot OH$ attack were taken from literature values or assigned a generic value in the range of (5×10^9) – (1×10^8) depending on the analogies between the compounds considered and other species whose kinetic constants are known.²⁵ Iron oxides and oxalate could trigger the Fenton-like oxidation process without additional H_2O_2 in the case of the intermediate role of oxalate generating $\cdot OH$ radicals. Almost 96% of phenol is degraded after 180 min in the described photocatalyst system, exhibiting efficient photocatalytic activity under visible-light irradiation.

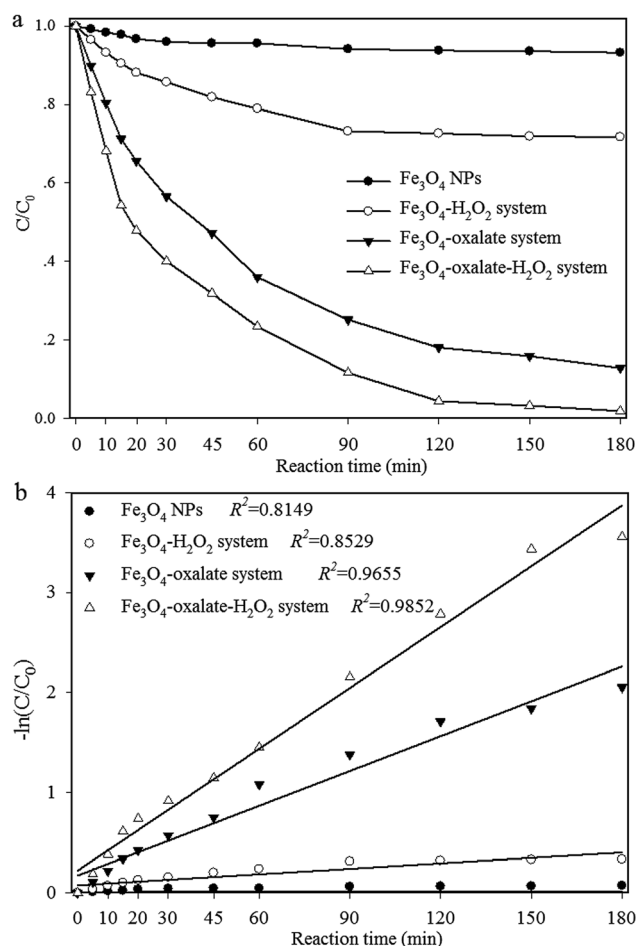


Fig. 7 (a) Time course of phenol degradation in a series of Fe_3O_4 based systems and (b) pseudo-first-order kinetics of phenol degradation (pH 2.0, oxalate 2.2 mM, time 3 h, initial phenol concentration 100 mg L^{-1}).

Phenol concentration *versus* the reaction time was further conducted by the equation of pseudo-first-order kinetics $\ln(C/C_0) = -kt$, where C_0 and C are the phenol concentrations in solution at times 0 and t , respectively, and k is the pseudo-first-order rate constant. Additionally, initial degradation rate is

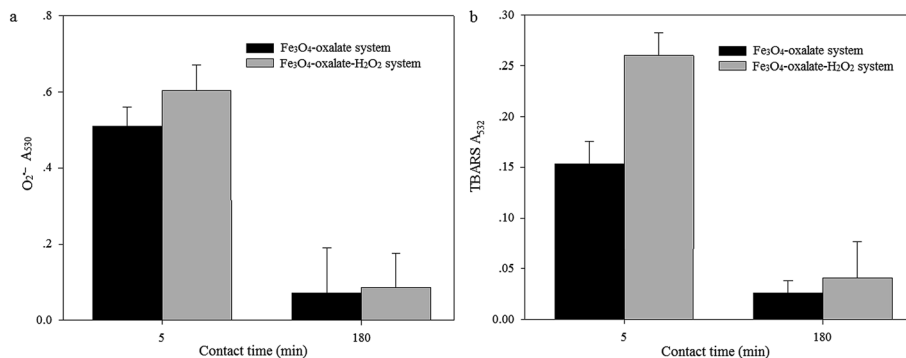


Fig. 6 Variation of $O_2^{\cdot-}$ and $\cdot OH$ radicals in Fe_3O_4 -oxalate and Fe_3O_4 -oxalate- H_2O_2 systems at the initial and end of the phenol photodegradation process (pH 2.0, Fe_3O_4 NPs 1.0 g L^{-1} , initial phenol concentration 100 mg L^{-1} , H_2O_2 dosage 0 and 0.118 mM , respectively).

expressed as the degradation rate at the beginning of irradiation ($r_{in} = kC_0$). The calculated values of the initial rate were used for a comparison of the efficiency of the photodegradation process under different reaction conditions. The data adequately fitted the pseudo-first order model in Fe_3O_4 -oxalate and Fe_3O_4 -oxalate- H_2O_2 system, with high correlation coefficients of 0.9655 and 0.9852, respectively (Fig. 7b). Pseudo-first-order rate constants were estimated as given in Table 2. The initial oxidation rate was accelerated from $0.03 \text{ mg L}^{-1} \text{ min}^{-1}$ to $1.83 \text{ mg L}^{-1} \text{ min}^{-1}$ by comparison between Fe_3O_4 NPs and Fe_3O_4 -oxalate systems. Furthermore, the addition of H_2O_2 into Fe_3O_4 -oxalate systems further accelerated the rate of phenol photodegradation because the exogenous H_2O_2 would promote the formation of $\cdot OH$ radicals. Meanwhile, the value of half-life, that is, the time required to decrease the concentration of the reactant to half the amount present before the reaction was also presented in Table 2. It is apparent that the half-time of Fe_3O_4 -oxalate and Fe_3O_4 -oxalate- H_2O_2 systems is much smaller than those of Fe_3O_4 nanoparticles.

3.6. Effect of Fe_3O_4 nanoparticles on phenol photodegradation

To test the effect of Fe_3O_4 nanoparticles on phenol degradation, the experiments were carried out in the suspension with an initial concentration of 50 mg L^{-1} phenol at pH 2.0 (Fig. 8). Fe_3O_4 NPs applied at the whole concentrations improved phenol removal, but the improvements were not closely proportional to the Fe_3O_4 NPs concentration elevation. Fig. 8 demonstrates that the increase of Fe_3O_4 NPs at the range of 0.1 – 1.0 g L^{-1} resulted in an elevation in phenol photodegradation, thereafter tend to be stationary in the presence of 2.0 to 4.0 g L^{-1} Fe_3O_4 NPs. When sufficient photocatalysts are available, the reaction rapidly proceeds to a decrease in phenol, ensuring a complete degradation of phenol. Fig. 7 also shows the iron species, $Fe(II)$ and $Fe(III)$ in the solution after 3 h of photodegradation in the presence of a series of concentration of Fe_3O_4 NPs. Apparently, the concentration of $Fe(II)$ and $Fe(III)$ depended strongly on the initial Fe_3O_4 NPs. A higher Fe_3O_4 dosage contributed to a higher concentration of $Fe(II)$ and $Fe(III)$ during phenol photodegradation process.

3.7. Effect of H_2O_2 on phenol photodegradation

It is widely reported that the involution of H_2O_2 is a critical issue of the Fenton and related oxidation processes. The effect of the use of H_2O_2 on the phenol degradation can be clearly observed in Fig. 9. The efficiency of the methods in terms of total phenol

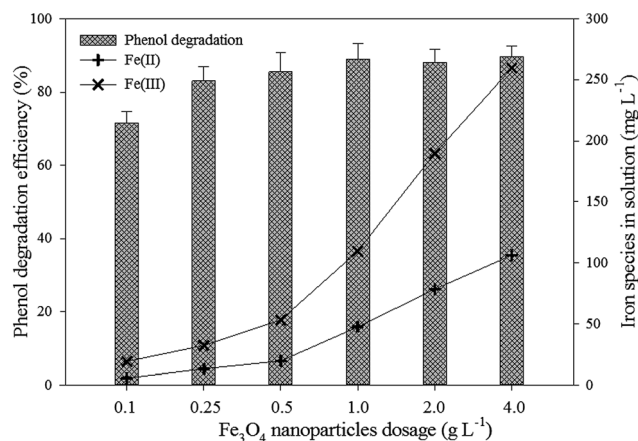


Fig. 8 Fe_3O_4 NPs dependent phenol degradation in Fe_3O_4 -oxalate system with various dosages of Fe_3O_4 NPs and speciation of $Fe(II)$ and $Fe(III)$ in the solution in the photodegradation process (pH 2.0, oxalate 2.2 mM , time 3 h, initial phenol concentration 100 mg L^{-1}).

removal reveals that the addition of H_2O_2 to the Fe_3O_4 -oxalate system enhances the organics conversion. By considering the evolution profiles of individual phenols, higher induction of phenol removal was observed when applying the promoted photocatalytic process; however, the continuous supply of H_2O_2 showed insignificant effect on phenol degradation, once a sufficient amount of radicals has been generated.

As inferred from Fig. 9, there is an optimum concentration of H_2O_2 . The highest efficiency of phenol degradation was obtained with the addition of 0.236 mM H_2O_2 , at the value of 98.70%. The auxo-action role of H_2O_2 involved in phenol degradation might occur in two possible pathways. On one hand, H_2O_2 can directly react with the parent compounds starting a chain mechanism in the presence of oxygen; on the other hand (most probable), H_2O_2 may decompose into $\cdot OH$ via the Fenton reaction. According to above equations, the photolysis of Fe_3O_4 -oxalate complexes forms H_2O_2 , endowing the acceptable degradation efficiency at the absence of H_2O_2 in Fe_3O_4 -oxalate photocatalysis via various pathways, for instance, electron trapping, thermal decomposition, reaction with superoxide radicals; moreover, the phenol conversion is enhanced by the participation of H_2O_2 . The increase of the photocatalytic rates with the exogenous addition of H_2O_2 can be attributed to the thermodynamically more favorable formation of $\cdot OH$ in the case of sufficient H_2O_2 supply. From the theoretical point of view, increasing the amount of H_2O_2 would eventually lead to a higher $\cdot OH$ generation through electron

Table 2 Pseudo-first-order kinetic constants for the photodegradation of phenol

Process	Rate constant k , min^{-1}	Initial oxidation rate ($\text{mg L}^{-1} \text{ min}$)	$t_{1/2}$ (h)	R^2
Fe_3O_4	0.0003	0.03	38.51	0.8141
Fe_3O_4 - H_2O_2	0.0017	0.17	6.80	0.8529
Fe_3O_4 -oxalate	0.0183	1.83	0.63	0.9655
Fe_3O_4 -oxalate- H_2O_2	0.0190	1.90	0.61	0.9852

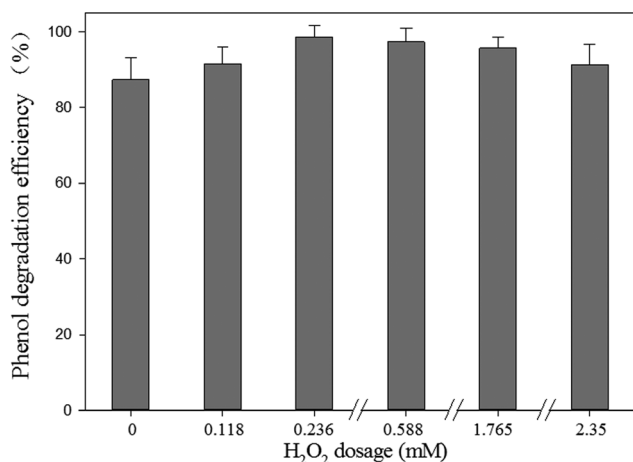
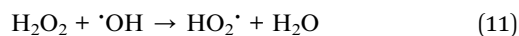
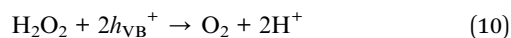


Fig. 9 H₂O₂-dependent phenol degradation and residual H₂O₂ concentration in Fe₃O₄ NPs–oxalate system with various dosages of H₂O₂ (pH 2.0, Fe₃O₄ NPs 1.0 g L⁻¹, oxalate 2.2 mM, time 3 h, initial phenol concentration 100 mg L⁻¹).

trapping or homogeneous scission. However, excessive H₂O₂ may lead to a decrease in phenol degradation. Even at high concentrations, H₂O₂ may become a scavenger of valence band holes and $\cdot\text{OH}$ (eqn (10) and (11)). Additionally, it has been reported that an excess of H₂O₂ concentration also involves an increase in its inefficient decomposition to yield oxygen and water instead of hydroxyl radicals.²⁵



3.8. Effect of initial phenol concentration

Fig. 10 illustrates the photodegradation efficiency at various initial phenol concentrations. Slight increases in phenol

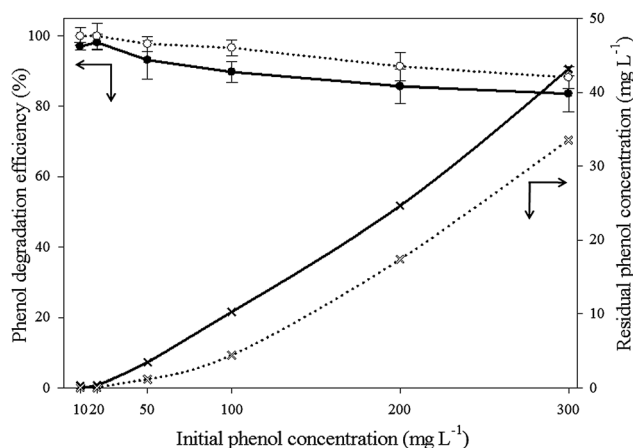


Fig. 10 Concentration-dependent phenol degradation and residual phenol concentrations in the presence of Fe₃O₄–oxalate and Fe₃O₄–oxalate–H₂O₂ system (pH 2.0, Fe₃O₄ NPs 1.0 g L⁻¹, oxalate 2.2 mM, time 3 h, H₂O₂ 0 and 0.236 mM, respectively).

photodegradation were observed by comparison with the Fe₃O₄–oxalate and Fe₃O₄–oxalate–H₂O₂ systems. It was found that the phenol removal efficiency almost remained stable of 99.9% when C₀ was less than 20 mg L⁻¹, and the highest phenol removal efficiency of 99.96% was obtained when C₀ was 20 mg L⁻¹ degraded by Fe₃O₄–oxalate–H₂O₂ system. With the continuous increase of phenol, a slight decrease occurred, based on the fact that the photodegradation process may be controlled by the limited numbers of surface sites of the photocatalyst with the excess phenol concentrations. The present results indicated that photocatalytic oxidation process is rather promising at low phenol concentrations, which is considered to be of a great importance in industrial applications.

4. Conclusions

In this work, Fe₃O₄–oxalate based photo-Fenton-like system performed photodegradation of phenol was studied. Fe₃O₄ NPs were prepared with the homogeneity dimensional size concentrated at diameters of approximately 12–20 nm. Photodegradation efficiency was highly pH dependent and decreased with an increase of pH in the range of 2.0–9.0. Independence of oxalate is proven to enhance the photocatalytic activity of the Fe₃O₄ NPs in the case of initiation of H₂O₂, which triggered the O₂^{•-} formation and $\cdot\text{OH}$ generation *via* Fenton reaction. Equilibrium data were well fitted by pseudo-first-order kinetic models. Moreover, an exogenous addition of H₂O₂ also enhanced the photodegradation of phenol, with the promoted formation of O₂^{•-} and $\cdot\text{OH}$. The optimal photodegradation condition occurred at pH 2.0 and at the concentration of 2.2 mM oxalate and 0.236 mM H₂O₂. Under the optimal conditions, 99.92% and 97.61% of phenol were removed at phenol concentration of 10 mg L⁻¹ and 100 mg L⁻¹, respectively. In conclusion, it appears that iron oxide nanomaterials are suitable for wastewater treatment through photodegradation and that more investigations are needed to design and optimize an industrial continuous process for phenol removal from wastewater.

Acknowledgements

The study was financially supported by the National Natural Science Foundation of China (51378190, 51039001, 51278176), the Hunan Provincial Innovation Foundation For Postgraduate (CX2013B152, CX2012B137), the Zhejiang Provincial Key Laboratory of solid Waste Treatment and Recycling open fun (SWTR-2012-07), the Environmental Protection Technology Research Program of Hunan (2007185), the New Century Excellent Talents in University (NCET-13-0186) and the Program for Changjiang Scholars and Innovative Research Team in University (IRT-13R17).

References

- 1 R. L. Qiu, D. D. Zhang, Z. H. Diao, X. F. Huang, C. He, J. L. Morel and Y. Xiong, *Water Res.*, 2012, **46**, 2299–2306.
- 2 G. M. Zeng, M. Chen and Z. T. Zeng, *Nature*, 2013, **499**, 154.

- 3 S. Esplugas, J. Gimenez, S. Contreras, E. Pascual and M. Rodríguez, *Water Res.*, 2002, **36**, 1034–1042.
- 4 M. A. Lazar and W. A. Daoud, *RSC Adv.*, 2013, **3**, 4130–4140.
- 5 Y. Li, J. Wang, H. Yao, L. Dang and Z. Li, *J. Mol. Catal. A: Chem.*, 2011, **334**, 116–122.
- 6 M. Pera-Titus, V. García-Molina, M. A. Banos, J. Giménez and S. Esplugas, *Appl. Catal., B*, 2004, **47**, 219–256.
- 7 W. Jiang, Q. Cai, W. Xu, M. Yang, Y. Cai, D. D. Dionysiou and K. E. O'Shea, *Environ. Sci. Technol.*, 2014, **48**, 8078–8085.
- 8 P. Xu, G. M. Zeng, D. L. Huang, C. L. Feng, S. Hu, M. H. Zhao, C. Lai, Z. Wei, C. Huang and G. X. Xie, *Sci. Total Environ.*, 2012, **424**, 1–10.
- 9 T. J. Liu, Q. Wang and P. Jiang, *RSC Adv.*, 2013, **3**, 12662–12670.
- 10 M. Yasui, K. Katagiri, S. Yamanaka and K. Inumaru, *RSC Adv.*, 2012, **2**, 11132–11137.
- 11 D. Vione, C. Minero, V. Maurino, M. E. Carlotti, T. Picatotto and E. Pelizzetti, *Appl. Catal., B*, 2005, **58**, 79–88.
- 12 X. W. Zhang and L. C. Lei, *Appl. Surf. Sci.*, 2008, **254**, 2406–2412.
- 13 S. A. C. Carabineiro, N. Bogdanchikova, P. B. Tavares and J. L. Figueiredo, *RSC Adv.*, 2012, **2**, 2957–2965.
- 14 M. Niu, F. Huang, L. Cui, P. Huang, Y. Yu and Y. Wang, *ACS Nano*, 2010, **4**, 681–688.
- 15 P. Xu, G. M. Zeng, D. L. Huang, C. Lai, M. H. Zhao, Z. Wei, N. J. Li, C. Huang and G. X. Xie, *Chem. Eng. J.*, 2012, **203**, 423–431.
- 16 J. L. Gong, B. Wang, G. M. Zeng, C. P. Yang, C. G. Niu, Q. Y. Niu, W. J. Zhou and Y. Liang, *J. Hazard. Mater.*, 2009, **164**, 1517–1522.
- 17 J. K. Leland and A. J. Bard, *J. Phys. Chem.*, 1987, **91**, 5076–5083.
- 18 X. H. Feng, H. J. Guo, K. Patel, H. Zhou and X. Lou, *Chem. Eng. J.*, 2014, **244**, 327–334.
- 19 G. Rothenberger, J. Moser, M. Graetzel, N. Serpone and D. K. Sharma, *J. Am. Chem. Soc.*, 1985, **107**, 8054–8059.
- 20 X. Zhong, S. Royer, H. Zhang, Q. Huang, L. Xiang, S. Valange and J. Barrault, *Sep. Purif. Technol.*, 2011, **80**, 163–171.
- 21 E. Bizani, K. Fytianos, I. Poullos and V. Tsiridis, *J. Hazard. Mater.*, 2006, **136**, 85–94.
- 22 Y. Zuo and J. Hoigne, *Environ. Sci. Technol.*, 1992, **26**, 1014–1022.
- 23 B. M. Voelker, F. M. Morel and B. Sulzberger, *Environ. Sci. Technol.*, 1997, **31**, 1004–1011.
- 24 P. Xu, G. Zeng, D. Huang, S. Hu, C. Feng, C. Lai, M. Zhao, C. Huang, N. Li and Z. Wei, *Colloids Surf., A*, 2013, **419**, 147–155.
- 25 N. J. Li, G. M. Zeng, D. L. Huang, S. Hu, C. L. Feng, M. H. Zhao, C. Lai, C. Huang, Z. Wei and G. X. Xie, *Bioresour. Technol.*, 2011, **102**, 8137–8142.
- 26 C. Paipa, E. Poblete and M. I. Toral, *Miner. Eng.*, 2006, **19**, 1465–1468.
- 27 M. Cheng, G. M. Zeng, D. L. Huang, L. Liu, M. H. Zhao, C. Lai, C. Huang, Z. Wei, N. J. Li, P. Xu, C. Zhang, F. L. Li and Y. Leng, *Biochem. Eng. J.*, 2014, **84**, 9–15.
- 28 F. J. Rivas, J. Frades, M. A. Alonso, C. Montoya and J. Monteagudo, *J. Agric. Food Chem.*, 2005, **53**, 10097–10104.
- 29 J. Lei, C. S. Liu, F. B. Li, X. M. Li, S. G. Zhou, T. X. Liu, M. H. Gu and Q. T. Wu, *J. Hazard. Mater.*, 2006, **137**, 1016–1024.
- 30 N. Quici, M. E. Morgada, G. Piperata, P. Babay, R. T. Gettar and M. I. Litter, *Catal. Today*, 2005, **101**, 253–260.
- 31 F. B. Li, J. J. Chen, C. S. Liu, J. Dong and T. X. Liu, *Biol. Fertil. Soils*, 2006, **42**, 409–417.
- 32 J. K. Leland and A. J. Bard, *J. Chem. Phys.*, 1987, **91**, 5076–5083.
- 33 C. Siffert and B. Sulzberger, *Langmuir*, 1991, **7**, 1627–1634.
- 34 C. Liu, F. Li, X. Li, G. Zhang and Y. Kuang, *J. Mol. Catal. A: Chem.*, 2006, **252**, 40–48.